


# Assessment of the Spatial Heterogeneity of Breast Cancers: Associations Between Computed Tomography and Immunohistochemistry

Biomarkers in Cancer  
Volume 11: 1–7  
© The Author(s) 2019  
Article reuse guidelines:  
sagepub.com/journals-permissions  
DOI: 10.1177/1179299X19851513



David K Woolf<sup>1,2</sup>, Sonia P Li<sup>1</sup>, Simone Detre<sup>3</sup>, Alison Liu<sup>4</sup>, Andrew Gogbashian<sup>5</sup>, Ian C Simcock<sup>5</sup>, James Stirling<sup>5</sup>, Michael Kosmin<sup>1</sup>, Gary J Cook<sup>4</sup> , Muhammad Siddique<sup>4</sup>, Mitch Dowsett<sup>3</sup>, Andreas Makris<sup>1</sup> and Vicky Goh<sup>4,5</sup>

<sup>1</sup>Breast Cancer Research Unit, Mount Vernon Cancer Centre, Northwood, UK.

<sup>2</sup>Department of Clinical Oncology, The Christie NHS Foundation Trust, Manchester, UK.

<sup>3</sup>Ralph Lauren Centre for Breast Cancer Research, Royal Marsden Hospital, London, UK.

<sup>4</sup>Division of Imaging Sciences, King's College London, St Thomas' Hospital, London, UK.

<sup>5</sup>Paul Strickland Scanner Centre, Mount Vernon Cancer Centre, Northwood, UK.

## ABSTRACT

**BACKGROUND:** Tumour heterogeneity is considered an important mechanism of treatment failure. Imaging-based assessment of tumour heterogeneity is showing promise but the relationship between these mathematically derived measures and accepted 'gold standards' of tumour biology such as immunohistochemical measures is not established.

**METHODS:** A total of 20 women with primary breast cancer underwent a research dynamic contrast-enhanced computed tomography prior to treatment with data being available for 15 of these. Texture analysis was performed of the primary tumours to extract 13 locoregional and global parameters. Immunohistochemical analysis associations were assessed by the Spearman rank correlation.

**RESULTS:** Hypoxia-inducible factor-1 $\alpha$  was correlated with first-order kurtosis ( $r = -0.533$ ,  $P = .041$ ) and higher order neighbourhood grey-tone difference matrix coarseness ( $r = 0.54$ ,  $P = .038$ ). Vascular maturity-related smooth muscle actin was correlated with higher order grey-level run-length long-run emphasis ( $r = -0.52$ ,  $P = .047$ ), fractal dimension ( $r = 0.613$ ,  $P = .015$ ), and lacunarity ( $r = -0.634$ ,  $P = .011$ ). Micro-vessel density, reflecting angiogenesis, was also associated with lacunarity ( $r = 0.547$ ,  $P = .035$ ).

**CONCLUSIONS:** The associations suggest a biological basis for these image-based heterogeneity features and support the use of imaging, already part of standard care, for assessing intratumoural heterogeneity.

**KEYWORDS:** Breast cancer, tumour heterogeneity, immunohistochemistry, computed tomography, texture analysis

**RECEIVED:** January 31, 2019. **ACCEPTED:** April 23, 2019.

**TYPE:** Original Research

**FUNDING:** The author(s) disclosed receipt of the following financial support for the research, authorship, and/or publication of this article: The authors are grateful to the Institute of Cancer Research Academic Partnership Challenge Fund, the Breast Cancer Campaign, and the Breast Cancer Research Trust for funding this study. They also acknowledge the support from the NIHR Biomedical Research Centre of Guy's and St Thomas' NHS Foundation Trust in partnership and King's College London and

UCL Comprehensive Cancer Imaging Centre funded by the CRUK and EPSRC in association with the MRC and DoH (England). The funders had no involvement in the study design, data collection and analysis, writing, or submission of the manuscript.

**DECLARATION OF CONFLICTING INTERESTS:** The author(s) declared no potential conflicts of interest with respect to the research, authorship, and/or publication of this article.

**CORRESPONDING AUTHOR:** David K Woolf, Breast Cancer Research Unit, Mount Vernon Cancer Centre, Northwood HA6 2RN, UK. Email: dwoolf@doctors.org.uk

## Introduction

It has been an aspiration that increasing knowledge of the biological mechanisms that underpin cancer development and progression will lead to improvements in individualized therapy for cancers. The characterization of cancers is normally performed via a biopsy, either from a primary or metastatic lesion. There is increasing awareness that these small samples may not be representative of the whole tumour, or of other metastases, in the same patient.<sup>1</sup> Tumoural heterogeneity may be responsible for treatment failures where therapy is directed against a specific molecular characteristic.<sup>2</sup> Previous work examining multiple tumour samples from the same patient has identified significant intratumoural genomic heterogeneity between geographic regions in the same tumour (spatial heterogeneity) as well as between the primary tumour and the local or distant disease (intertumoural heterogeneity).<sup>3,4</sup> Established receptor status

such as oestrogen receptor (ER), progesterone receptor (PR), and human epidermal growth factor receptor-2 (HER-2) have been shown to have considerable discordance in the same primary tumours, between primary and secondary tumours and also over time.<sup>5</sup> In addition, distinct populations of subclones can also vary throughout the course of the disease due to disease progression or metastasis or as a result of outside influences such as drug therapy (temporal heterogeneity).<sup>6,7</sup>

There is increasing awareness that non-invasive imaging may have a role in assessing tumour heterogeneity.<sup>8</sup> Imaging is already used widely in the management of a cancer patient including diagnosis, staging, assessment of treatment response, and surveillance. Computed tomography (CT) is well placed for tumour heterogeneity assessment as it is routinely used in clinical practice as the standard of care for cancer staging and response assessment and thus is cost effective. Computed



tomography images are of high resolution (typically 0.7 mm × 0.7 mm in plane pixel size) allowing the spatial heterogeneity to be quantified by image analysis that provides both global (whole tumour) or locoregional (inter-pixel) measure of the distribution and spatial characteristics of pixel signal intensity within the tumour using statistical (first, second, or higher order) or model-based mathematical methods.<sup>9</sup> It is clear from visual inspection of medical images, for example, CT, magnetic resonance imaging (MRI), and positron emission tomography (PET), that there are phenotypical spatial (and temporal) differences in Hounsfield units, signal intensity, or tracer uptake – so-called ‘imaging heterogeneity’. In the last few years, there has been increasing number of studies supporting the hypothesis that the phenotypic patterns on imaging reflect biological heterogeneity, for example, differences in angiogenesis, hypoxia, or gene expression. An increasing number of studies have also confirmed that imaging measures have an impact on outcome, for example, survival, relapse, or response to therapy. How these heterogeneity parameters relate to key biological tumour processes (angiogenesis, hypoxia, and proliferation) is an area of intense research interest.

A total of 4 key studies in renal cell cancer, non-small cell lung cancer, colorectal cancer, and oesophageal cancer have demonstrated the associations between angiogenic factors, hypoxic markers and proliferation and PET, PET/MRI, MRI and CT parameters.<sup>10–13</sup> Radiogenomics, the use of quantitative data from imaging combined with clinical and patient-centred data, has been recognized as playing a potentially central role in the future for a personalized medical approach in breast cancer.<sup>14</sup> A number of studies have looked at a wide range of molecular data such as oestrogen status, HER-2,<sup>15</sup> gene expression analysis<sup>16</sup> and multigene assays such as Oncotype DX<sup>17</sup> and proliferation markers.<sup>18–20</sup> These studies have looked at the relationships with a number of imaging techniques including dynamic contrast-enhanced magnetic resonance imaging (DCE-MR)<sup>21</sup> and <sup>18</sup>fluorodeoxyglucose positron emission tomography (FDG-PET)<sup>22,23</sup> and found a number of correlations that have the potential to be incorporated into future prospective studies for confirmation. Another specific tool under investigation has been the use of non-invasive imaging techniques such as PET using radiolabeled antibodies and in particular HER-2 PET/CT to help predict patient benefit from HER-2-directed therapies.<sup>24–30</sup>

Angiogenesis plays a driving role in cancer development and progression<sup>31,32</sup> and has been defined as one of the hallmarks of cancer.<sup>33</sup> Data from breast cancer show that angiogenesis in the primary cancer can predict for disease-free and overall survival.<sup>34–40</sup> Vascular endothelial growth factor (VEGF) is a vital member of a group of cytokines that play a critical role in angiogenesis. Of particular note, it increases microvascular permeability, induces endothelial cell migration, division, and survival as well as inducing angiogenesis through a variety of mechanisms.<sup>41,42</sup>

Hypoxia-inducible factor-1 $\alpha$  (Hif-1 $\alpha$ ) is also a key transcription factor, induced by hypoxia, that can stimulate angiogenic factors including VEGF, proliferation, and cell-adhesion genes.<sup>43</sup> Hypoxia also activates carbonic anhydrase IX (CAIX) activity which is thought to reduce the pH of tumours thus increasing their growth and survival ability<sup>43,44</sup>; it is a marker of poor prognosis in breast cancer.<sup>45</sup> Glucose transporter-1 (GLUT-1), also regulated by Hif-1 $\alpha$ , mediates cellular glucose uptake, which is an important part of cell proliferation and is required for tumour cell maintenance and growth.<sup>46</sup> It is over-expressed in many tumours and associated with poorer survival. Ki-67 provides a measure of cell proliferation and is a prognostic marker in breast cancer.<sup>47,48</sup>

Our hypothesis is that image-based heterogeneity is associated with hypoxia, angiogenesis, and proliferation. This prospective study aimed to examine the relationship between contrast-enhanced CT parameters and the accepted gold standard immunohistochemical (IHC) biological markers of angiogenesis, hypoxia, and proliferation in breast cancer.

## Methods

### Patients

A total of 20 women with histologically proven primary breast tumours were recruited from January 2009 to August 2010 and underwent a DCE-CT prior to treatment with neoadjuvant chemotherapy (NAC). Following NAC, patients then went on to receive surgery as standard of care, either mastectomy or breast-conserving surgery with an appropriate axillary procedure (usually axillary nodal dissection). Institutional review board approval was obtained for this study (08/H0311/147) and all patients gave written consent to participate in this sub-study of a previously published study.<sup>49</sup>

### Computed tomography acquisition and analysis

Dynamic contrast-enhanced CT (SOMATOM Definition, Siemens Healthcare, Forchheim, Germany) was performed following intravenous iodinated contrast agent (50 mL ioversol 350 mg/mL iodine at 6 mL/s; Optiray; Covidien, Mansfield, MA, USA) using a 4-dimensional (4D) adaptive spiral technique (80 kV, 100–120 mAs, 0.33 seconds rotation time, matrix 512 × 512, scan field of view 300–450 mm, and reconstructed slice thickness 3 mm with 2 mm increment). Heterogeneity analysis was performed on the final enhancement phase axial images, 50-second post-intravenous contrast injection, using in-house software implemented with MATLAB (MathWorks, Natick, MA, USA). Following application of a smoothing filter, a volume of interest (VOI) was created for the entire primary tumour by outlining the whole tumour on all axial images where visible by 2 observers in consensus (with 1 and >15 years of CT experience). Global texture features were calculated for the whole tumour volume using (1) first-order statistical histogram methods (mean, skewness, kurtosis, energy, and entropy)

and (2) model-based fractal analysis (fractal dimension and lacunarity). Locoregional texture features, examining the individual inter-pixel relationships, were calculated using (1) second-order statistical (grey-level co-occurrence matrix [GLCM]: energy) and (2) higher order statistical methods (neighbourhood grey tone-difference matrix [NGTDM]: coarseness, contrast, busyness; grey-level run length [GLRL]: long run emphasis; grey-level size zone matrix [GLSZM]: long zone emphasis) (see Supplementary Material for parameter definitions and equations). These were selected from their usage in previous publications and likely clinical relevance.<sup>9,50</sup>

### Immunohistochemistry

All IHC procedures were performed on the core biopsies obtained for diagnosis; the formalin-fixed paraffin-embedded (FFPE) sections were de-waxed with xylene and brought to the aqueous phase with decreasing concentrations of industrialized methylated spirits. The 3,3'-diaminobenzidine (DAB) chromogen was used to provide the brown-coloured end-product staining visualized under a bright-field microscope. The negative controls comprised the known positive control tissue incubated with diluent under the same conditions at the same time as the test samples. The pretreatment methods are described as below.

**Ki-67.** Antigen retrieval was carried out by microwaving the sections in pH 6 citrate buffer. Using the Dako Autostainer (Dako Ltd., Cambs, UK) with REAL Kit, the sections were incubated with monoclonal mouse anti-human Ki-67 antigen clone MIB-1 (Dako) at 1/50 dilution for 20 minutes. Scoring of at least 500 invasive breast cancer cell nuclei in 5 high-power fields (HPFs) at  $\times 400$  magnification was carried out to obtain a percentage positive score. If 500 cells were not available in 5 HPFs, more fields were scored to achieve this. The control used was a previously validated Ki-67 positive tissue microarray.

**Smooth muscle actin.** No pretreatment antigen retrieval was needed. Avidin/biotin block was applied prior to application of anti-smooth muscle actin (SMA) monoclonal mouse antibody clone 1A4 at a dilution of 1/300 and using the Dako REAL Kit. A ductal carcinoma in situ (DCIS) breast cancer known to be positive for SMA was used as the control. The number of large vessels stained brown/HPF were recorded.

**Carbonic anhydrase IX.** No pretreatment was required. A serum-free protein block (Dako) was applied prior to incubating with anti-CAIX polyclonal antibody clone M75 (Abcam, Cambridge, UK) at 1/1000 dilution for 1 hour using the Dako EnVision FLEX+ Kit on a Dako Autostainer. Stomach tissue known to be positive for CAIX was used for the control. Scoring was by a modified H score which estimated by eye the percentage cytoplasmic positive invasive tumour and 0, 1+, 2+, and 3+ staining intensity as an average calculated from the 10 HPFs assessed.

**CD34 (micro-vessel density).** No pretreatment was required. Monoclonal mouse anti-CD34 (Class II Clone QBend 10; Dako) ready-to-use undiluted was used with the Dako EnVision FLEX+ Kit. Placenta tissue known to be positive for this biomarker was used as the control. The number of vessels staining positive per HPF was estimated by eye and the average taken from 10 HPFs was the resultant score.

**Glucose transporter-1.** Pretreatment of the sections was carried out for 30 minutes in a water bath at 97°C in low pH Flex antigen retrieval solution. Sections were incubated for 20 minutes with 1/600 anti-human GLUT-1 mouse monoclonal antibody (Abcam SPM498). Dako EnVision FLEX+ Kit was used and liver was the control tissue. Percentage membrane positive staining per HPF was estimated from an average of 10 HPFs assessed.

**Vascular endothelial growth factor.** Antigen retrieval was carried out by microwaving the sections for 18 minutes in pH 6 citrate buffer. Serum-free protein block (Dako) was applied prior to incubation of the sections with 1/400 mouse monoclonal anti-VEGF (VG-1) antibody (Abcam 1316) for 1 hour. The Dako EnVision FLEX+ Kit was used thereon. Human breast angiosarcoma and pancreas were used as control tissue. The percentage positive cytoplasmic staining cells and the overall intensity of their staining were estimated, and this was used for the purposes of statistical analysis. The intensity was described as weak, moderate, or strong.

**Hypoxia-inducible factor-1 $\alpha$ .** Pretreatment of the sections was carried out for 30 minutes in a water bath at 97°C in high pH Flex antigen retrieval solution. The sections were incubated in 1/200 mouse monoclonal Hif-1 $\alpha$  subunit antibody (BD Biosciences, Wokingham, UK) for 20 minutes using the Dako Autostainer and EnVision FLEX+ Kit. A comedo breast cancer core-cut known to be positive was used as control tissue. Scoring was by a modified H score which estimated by eye the percentage nuclear positive invasive tumour which was used for the statistical analysis and 0, 1+, 2+, and 3+ staining intensity as an average calculated from the 10 HPFs assessed.

### Statistical analysis

Correlation of the CT heterogeneity parameters with IHC scores was performed using the Spearman rank correlation coefficient, as the sample size was small and non-symmetrically distributed. Correlations between IHC scores were also assessed using the Spearman rank correlation coefficient. In this exploratory analysis, statistical significance was defined as a 2-tailed *P*-value of less than .05.

## Results

### Patients

All 20 CT studies were analysed successfully but only 15 patients had an immunohistochemistry outcome; 3 patients

**Table 1.** Baseline patient demographics and tumour characteristics.

Median age at diagnosis (range)	46.9 (35.5-80)
Premenopausal	11 (73%)
Postmenopausal	1 (7%)
Perimenopausal	1 (7%)
Unevaluable	2 (13%)
Invasive ductal carcinoma	13 (87%)
Mixed invasive ductal and lobular carcinoma	1 (7%)
Other or not otherwise specified	1 (7%)
Grade II	6 (40%)
Grade III	8 (53%)
Grade not otherwise specified	1 (7%)
T1	1 (7%)
T2	7 (47%)
T3	6 (40%)
T4	1 (7%)
Node positive	11 (73%)
Node negative	4 (27%)
Oestrogen receptor positive	8 (53%)
Oestrogen receptor negative	7 (47%)
Progesterone receptor positive	5 (33%)
Progesterone receptor negative	10 (66%)
HER-2 positive	4 (27%)
HER-2 negative	11 (73%)

had insufficient material to be able to perform further immunohistochemistry testing, and biopsies for 2 patients were unable to be retrieved for further IHC analysis by the laboratory. We therefore report the data for these 15 patients. Baseline patient demographics, tumour characteristics, and clinical outcomes are shown in Table 1.

#### *Association between CT heterogeneity analysis and IHC*

There were a number of significant associations (Table 2; Appendix 1). Hypoxia-related Hif-1 $\alpha$  correlated negatively with global kurtosis ( $r=-0.533$ ,  $P=.041$ ) and positively with locoregional coarseness ( $r=0.54$ ,  $P=.038$ ) and long zone emphasis ( $r=0.54$ ,  $P=.038$ ). Smooth muscle actin correlated negatively with locoregional run-length long-run emphasis ( $r=-0.52$ ,  $P=.047$ ) and global lacunarity ( $r=-0.634$ ,  $P=.011$ ) and positively with global fractal dimension ( $r=0.613$ ,  $P=.015$ ). CD34 micro-vessel density (MVD) was also associated positively with global lacunarity ( $r=0.547$ ,  $P=.035$ ). No associations

**Table 2.** Significant correlations between CT heterogeneity analysis and IHC.

IHC FACTOR	CT HETEROGENEITY FACTOR	R-VALUE	P-VALUE
Hif-1 $\alpha$	Global kurtosis	-0.533	.041
	Locoregional coarseness	0.54	.038
	Long zone emphasis	0.54	.038
SMA	Locoregional run-length long-run emphasis	-0.52	.047
	Global lacunarity	-0.634	.011
	Global fractal dimension	0.613	.015
CD34-MVD	Global lacunarity	0.547	.035

Abbreviations: CT, computed tomography; IHC, immunohistochemical; MVD, micro-vessel density; SMA, smooth muscle actin.  $r$  is the Spearman correlation coefficient value;  $P$  is the significance value attached to the Spearman correlation coefficient value.

were found with Ki-67 (proliferation), VEGF (angiogenesis), GLUT-1, and CAIX (hypoxia).

#### *Associations between IHC parameters*

Correlation of the IHC results with each other revealed a significant correlation between GLUT-1 and CAIX ( $r=0.659$ ,  $P=.007$ ), GLUT-1 and MVD (CD34;  $r=-0.535$ ,  $P=.04$ ), and SMA and MVD (CD34;  $r=-0.546$ ,  $P=.035$ ) (see Supplementary Material S2).

## Discussion

In recent years, there have been an increasing number of CT studies that suggested that imaging heterogeneity may be an important predictive and prognostic biomarker.<sup>51,52</sup> In this exploratory study, we investigated the associations between primary breast CT image heterogeneity features with IHC markers of underlying tumour biology to inform on further directions of study. While there are a large number of features that can be extracted from an image, we selected a number of standard features, both global and locoregional, that have been reported on in previous publications and found to be clinically relevant.<sup>9,50,53</sup>

Our study findings suggest that there may indeed be a biological basis to image heterogeneity. Our study found that a number of primary breast CT heterogeneity features correlated with SMA and CD34-MVD as well as Hif-1 $\alpha$  suggesting that these features may provide some information regarding underlying vascular heterogeneity. Our study complements data from a previous study correlating CT first-order features with hypoxia and angiogenesis in non-small cell lung cancer.<sup>53</sup> CD34-MVD provides an indication of the distribution of microvessels within a tumour. Smooth muscle actin is expressed by activated fibroblasts (myofibroblasts) and also vascular



smooth muscle cells, pericytes, and myoepithelial cells<sup>54</sup> and reflects functional vessel maturity.

In particular, higher image fractal lacunarity, which is a measure of structural heterogeneity within an object, was associated with higher CD34-MVD but lower SMA indicating a relationship with angiogenesis and also areas of lower vessel maturity (lower SMA expression). There was also a positive association between fractal dimension and SMA expression, indicating an association between the spatial regularity within the tumour and increasing vessel maturity. The associations with Hif-1 $\alpha$  were also logical in the light of associations with SMA and CD34-MVD. Hif-1 $\alpha$  was negatively associated with kurtosis indicating hypoxia is associated with a tendency for platykurtosis, that is, a flatter peak with a negative kurtosis value. On a locoregional level, hypoxia was associated with higher coarseness and run emphasis, that is, greater locoregional heterogeneity.

Previous work has shown that the incorporation of spatial heterogeneity analysis with diffusion weighted (DW) and DCE-MRI may differentiate breast cancer by histological and molecular subtypes.<sup>55–57</sup> The use of MRI spatial heterogeneity data has also shown an improvement in the ability to predict response to NAC in breast cancers both in mouse models<sup>58</sup> and humans.<sup>56,59</sup> It has also been shown to correlate with Oncotype DX (Genomic Health, Redwood City, CA) recurrence scores,<sup>60</sup> which uses mRNA expression of a 21-gene panel, and is both predictive and prognostic of the outcomes for breast cancer and is widely used in clinical practice to quantify the benefit of adjuvant chemotherapy.<sup>61</sup> Our data add to the literature in supporting a biological basis for CT image heterogeneity and opens the potential for such analysis in the metastatic setting where CT is performed for diagnosis and response assessment.

We acknowledge that our study has a number of limitations. As previously discussed, the number of patients studied in our study was small, although comparable to other similar radiologic-pathologic correlative studies. The patient population also included variation in the traditional IHC markers such as grade, ER, and HER-2 status (Table 1). The immunohistochemistry samples were taken at baseline for correlation with the CT parameters rather than the post-operative specimen. This was necessary in a neoadjuvant setting as the post-operative specimen will be post-chemotherapy, but there are well-known sampling issues with core biopsies which may not represent the heterogeneity of the whole tumour.<sup>62</sup> We also had a relatively high ‘dropout’ rate as we were unable to analyse the core samples in 5 of the original 20 patients for the purposes of this study (25%). Acquisition parameters are known to affect CT texture analysis with kilovoltage and pixel size having a greater effect than milliampere (mA). In our study, we fixed these parameters so as to minimize the variability of the acquisition technique as our focus was the association of the parameters with IHC. Finally, multiple statistical testing was undertaken as part of this exploratory study which is acceptable practice but raises the possibility of type I errors.

In summary, the associations in our study between image heterogeneity features and CD34-MVD, SMA, and Hif-1 $\alpha$  suggest a biological basis for these image features and support further investigation to confirm these preliminary findings.

## Acknowledgements

The authors thank Frances Daley for her help and advice with the immunohistochemical techniques. They are grateful to the Institute of Cancer Research Academic Partnership Challenge Fund, the Breast Cancer Campaign, and the Breast Cancer Research Trust for funding this study. They also acknowledge the support from the NIHR Biomedical Research Centre of Guy’s and St Thomas’ NHS Foundation Trust in partnership and King’s College London and UCL Comprehensive Cancer Imaging Centre funded by the CRUK and EPSRC in association with the MRC and DoH (England). The funders had no involvement in the study design, data collection and analysis, writing, or submission of the manuscript.

## Author Contributions

All authors have made a substantial contribution to this study and approved the manuscript.

## Ethical Approval

This study has been approved by the appropriate ethics committee and has therefore been performed in accordance with the ethical standards laid down in the 1964 Declaration of Helsinki and its later amendments.

## Informed Consent

All patients gave their informed consent to the study.

## SUPPLEMENTAL MATERIAL

Supplemental material for this article is available online.

## ORCID iD

Gary J Cook  <https://orcid.org/0000-0002-8732-8134>

## REFERENCES

1. Song J-L, Chen C, Yuan J-P, Sun S-R. Progress in the clinical detection of heterogeneity in breast cancer. *Cancer Med*. 2016;5:3475–3488.
2. Yap TA, Gerlinger M, Futreal PA, Pusztai L, Swanton C. Intratumor heterogeneity: seeing the wood for the trees. *Science Translational Med*. 2012;4:10.
3. Bedard PL, Hansen AR, Ratain MJ, Siu LL. Tumour heterogeneity in the clinic. *Nature*. 2013;501:355–364.
4. Burrell RA, McGranahan N, Bartek J, Swanton C. The causes and consequences of genetic heterogeneity in cancer evolution. *Nature*. 2013;501:338–345.
5. Aurilio G, Disalvatore D, Pruneri G, et al. A meta-analysis of oestrogen receptor, progesterone receptor and human epidermal growth factor receptor 2 discordance between primary breast cancer and metastases. *Euro J Cancer*. 2014;50:277–289.
6. Klein CA. Selection and adaptation during metastatic cancer progression. *Nature*. 2013;501:365–372.
7. Shah SP, Morin RD, Khattra J, et al. Mutational evolution in a lobular breast tumour profiled at single nucleotide resolution. *Nature*. 2009;461:809–813.
8. Donners R, Blackledge M, Tunariu N, Messiou C, Merkle E, Koh D-M. Quantitative whole-body diffusion-weighted MR imaging. *Magn Reson Imaging Clin N Am*. 2018;26:479–494.

9. Davnall F, Yip CSP, Ljungqvist G, et al. Assessment of tumor heterogeneity: an emerging imaging tool for clinical practice. *Insights Imaging*. 2012;3:573–589.
10. Yin Q, Hung SC, Wang L, et al. Associations between tumor vascularity, vascular endothelial growth factor expression and PET/MRI radiomic signatures in primary clear-cell-renal-cell-carcinoma: proof-of-concept study. *Sci Rep*. 2017;7:43356.
11. Mandeville HC, Ng QS, Daley FM, et al. Operable non-small cell lung cancer: correlation of volumetric helical dynamic contrast-enhanced CT parameters with immunohistochemical markers of tumor hypoxia. *Radiology*. 2012;264:581–589.
12. Miles KA, Ganeshan B, Rodriguez-Justo M, et al. Multifunctional imaging signature for V-KI-RAS2 Kirsten rat sarcoma viral oncogene homolog (KRAS) mutations in colorectal cancer. *J Nucl Med*. 2014;55:386–391.
13. Yip C, Weeks A, Shaw K, et al. Magnetic resonance imaging (MRI) of intratumoral voxel heterogeneity as a potential response biomarker: assessment in a HER2+ esophageal adenocarcinoma xenograft following trastuzumab and/or cisplatin therapy. *Transl Oncol*. 2017;10:459–467.
14. Pinker K, Chin J, Melsaether AN, Morris EA, Moy L. Precision medicine and radiogenomics in breast cancer: new approaches toward diagnosis and treatment. *Radiology*. 2018;287:732–747.
15. Li H, Zhu Y, Burnside ES, et al. Quantitative MRI radiomics in the prediction of molecular classifications of breast cancer subtypes in the TCGA/TCIA data set. *NPJ Breast Cancer*. 2016;2:16012.
16. Yamamoto S, Maki DD, Korn RL, Kuo MD. Radiogenomic analysis of breast cancer using MRI: a preliminary study to define the landscape. *AJR Am J Roentgenol*. 2012;199:654–663.
17. Li H, Zhu Y, Burnside ES, et al. MR imaging radiomics signatures for predicting the risk of breast cancer recurrence as given by research versions of Mamma-Print, Oncotype DX, and PAM50 gene assays. *Radiology*. 2016;281:382–391.
18. Juan MW, Yu J, Peng GX, Jun LJ, Feng SP, Fang LP. Correlation between DCE-MRI radiomics features and Ki-67 expression in invasive breast cancer. *Oncol Lett*. 2018;16:5084–5090.
19. Ma W, Ji Y, Qi L, Guo X, Jian X, Liu P. Breast cancer Ki67 expression prediction by DCE-MRI radiomics features. *Clin Radiol*. 2018;73:909.e1–909.e5.
20. Liang C, Cheng Z, Huang Y, et al. An MRI-based radiomics classifier for preoperative prediction of Ki-67 status in breast cancer. *Acad Radiol*. 2018;25:1111–1117.
21. Yamamoto S, Han W, Kim Y, et al. Breast cancer: radiogenomic biomarker reveals associations among dynamic contrast-enhanced MR imaging, long non-coding RNA, and metastasis. *Radiology*. 2015;275:384–392.
22. Ha S, Park S, Bang JI, Kim EK, Lee HY. Metabolic radiomics for pretreatment 18F-FDG PET/CT to characterize locally advanced breast cancer: histopathologic characteristics, response to neoadjuvant chemotherapy, and prognosis. *Sci Rep*. 2017;7:1556.
23. Huang SY, Franc BL, Harnish RJ, et al. Exploration of PET and MRI radiomic features for decoding breast cancer phenotypes and prognosis. *NPJ Breast Cancer*. 2018;4:24.
24. Gebhart G, Lamberts LE, Wimana Z, et al. Molecular imaging as a tool to investigate heterogeneity of advanced HER2-positive breast cancer and to predict patient outcome under trastuzumab emtansine (T-DM1): the ZEPHIR trial. *Ann Oncol*. 2016;27:619–624.
25. Ulaner GA, Hyman DM, Ross DS, et al. Detection of HER2-positive metastases in patients with HER2-negative primary breast cancer using 89Zr-trastuzumab PET/CT. *J Nucl Med*. 2016;57:1523–1528.
26. Dehdashti F, Wu N, Bose R, et al. Evaluation of [89Zr]trastuzumab-PET/CT in differentiating HER2-positive from HER2-negative breast cancer. *Breast Cancer Res Treat*. 2018;169:523–530.
27. Lee H, Lee DE, Park S, et al. Predicting response to neoadjuvant chemotherapy in patients with breast cancer: combined statistical modeling using clinicopathological factors and FDG PET/CT texture parameters. *Clin Nucl Med*. 2019;44:21–29.
28. Magometschnigg H, Pinker K, Helbich T, et al. PIK3CA mutational status is associated with high glycolytic activity in ER+/HER2- early invasive breast cancer: a molecular imaging study using [18F]FDG PET/CT [published online ahead of print January 16, 2016]. *Mol Imaging Biol*. doi:10.1007/s11307-018-01308-z.
29. Zhao Y, Liu C, Zhang Y, et al. Prognostic value of tumor heterogeneity on 18F-FDG PET/CT in HR+HER2- metastatic breast cancer patients receiving 500 mg fulvestrant: a retrospective study. *Sci Rep*. 2018;8:14458.
30. De Cremoux P, Biard L, Poirot B, et al. 18FDG-PET/CT and molecular markers to predict response to neoadjuvant chemotherapy and outcome in HER2-negative advanced luminal breast cancer patients. *Oncotarget*. 2018;9:16343–16353.
31. Folkman J. How is blood vessel growth regulated in normal and neoplastic tissue? G.H.A. Clowes memorial Award lecture. *Cancer Res*. 1986;46:467–473.
32. Folkman J. Angiogenesis in cancer, vascular, rheumatoid and other disease. *Nat Med*. 1995;1:27–31.
33. Hanahan D, Weinberg RA. The hallmarks of cancer. *Cell*. 2000;100:57–70.
34. Weidner N, Semple JP, Welch WR, Folkman J. Tumor angiogenesis and metastasis – correlation in invasive breast carcinoma. *N Engl J Med*. 1991;324:1–8.
35. Horak ER, Leek R, Klenk N, et al. Angiogenesis, assessed by platelet/endothelial cell adhesion molecule antibodies, as indicator of node metastases and survival in breast cancer. *Lancet*. 1992;340:1120–1124.
36. Fox SB, Leek RD, Smith K, Hollyer J, Greenall M, Harris AL. Tumor angiogenesis in node-negative breast carcinomas – relationship with epidermal growth factor receptor, estrogen receptor, and survival. *Breast Cancer Res Treat*. 1994;29:109–116.
37. Gasparini G, Weidner N, Bevilacqua P, et al. Tumor microvessel density, p53 expression, tumor size, and peritumoral lymphatic vessel invasion are relevant prognostic markers in node-negative breast carcinoma. *J Clin Oncol*. 1994;12:454–466.
38. Gasparini G, Toi M, Gion M, et al. Prognostic significance of vascular endothelial growth factor protein in node-negative breast carcinoma. *J Natl Cancer Inst*. 1997;89:139–147.
39. Linderholm B, Grankvist K, Wilking N, Johansson M, Tavelin B, Henriksson R. Correlation of vascular endothelial growth factor content with recurrences, survival, and first relapse site in primary node-positive breast carcinoma after adjuvant treatment. *J Clin Oncol*. 2000;18:1423–1431.
40. Van den Eynden GG, Van der Auwera I, Van Laere SJ, et al. Angiogenesis and hypoxia in lymph node metastases is predicted by the angiogenesis and hypoxia in the primary tumour in patients with breast cancer. *Br J Cancer*. 2005;93:1128–1136.
41. Dvorak HF. Vascular permeability factor/vascular endothelial growth factor: a critical cytokine in tumor angiogenesis and a potential target for diagnosis and therapy. *J Clin Oncol*. 2002;20:4368–4380.
42. Brown LF, Berse B, Jackman RW, et al. Expression of vascular permeability factor (vascular endothelial growth factor) and its receptors in breast cancer. *Hum Pathol*. 1995;26:86–91.
43. Harris AL. Hypoxia—a key regulatory factor in tumour growth. *Nat Rev Cancer*. 2002;2:38–47.
44. Wykoff CC, Beasley NJ, Watson PH, et al. Hypoxia-inducible expression of tumor-associated carbonic anhydrases. *Cancer Res*. 2000;60:7075–7083.
45. Chia SK, Wykoff CC, Watson PH, et al. Prognostic significance of a novel hypoxia-regulated marker, carbonic anhydrase IX, in invasive breast carcinoma. *J Clin Oncol*. 2001;19:3660–3668.
46. Szablewski L. Expression of glucose transporters in cancers. *Biochim Biophys Acta*. 2013;1835:164–169.
47. Sheri A, Dowsett M. Developments in Ki67 and other biomarkers for treatment decision making in breast cancer. *Ann Oncol*. 2012;23:x219–x227.
48. Inwald EC, Klinkhammer-Schalke M, Hofstädter F, et al. Ki-67 is a prognostic parameter in breast cancer patients: results of a large population-based cohort of a cancer registry. *Breast Cancer Res Treat*. 2013;139(2):539–552.
49. Li SP, Makris A, Gogbashian A, Simcock IC, Stirling JJ, Goh V. Predicting response to neoadjuvant chemotherapy in primary breast cancer using volumetric helical perfusion computed tomography: a preliminary study. *Eur Radiol*. 2012;22:1871–1880.
50. Ganeshan B, Miles KA. Quantifying tumour heterogeneity with CT. *Cancer Imaging*. 2013;13:140–149.
51. Zhang H, Graham CM, Elci O, et al. Locally advanced squamous cell carcinoma of the head and neck: CT texture and histogram analysis allow independent prediction of overall survival in patients treated with induction chemotherapy. *Radiology*. 2013;269:801–809.
52. Yip C, Landau D, Kozarski R, et al. Primary esophageal cancer: heterogeneity as potential prognostic biomarker in patients treated with definitive chemotherapy and radiation therapy. *Radiology*. 2014;270:141–148.
53. Ganeshan B, Goh V, Mandeville HC, Ng QS, Hoskin PJ, Miles KA. Non-small cell lung cancer: histopathologic correlates for texture parameters at CT. *Radiology*. 2013;266:326–336.
54. Kalluri R, Zeisberg M. Fibroblasts in cancer. *Nat Rev Cancer*. 2006;6:392–401.
55. Waugh SA, Purdie CA, Jordan LB, et al. Magnetic resonance imaging texture analysis classification of primary breast cancer. *Eur Radiol*. 2015;26:322–330.
56. Chaudhury B, Zhou M, Goldgof DB, et al. Heterogeneity in intratumoral regions with rapid gadolinium washout correlates with estrogen receptor status and nodal metastasis. *J Magn Reson Imaging*. 2015;42:1421–1430.
57. Li H, Lan L, Drukker K, Perou C, Giger M. TU-AB-BRA-08: radiomics in the analysis of breast cancer heterogeneity on DCE-MRI. *Med Phys*. 2015;42:3588.
58. Longo DL, Dastrù W, Consolino L, et al. Cluster analysis of quantitative parametric maps from DCE-MRI: application in evaluating heterogeneity of tumor response to antiangiogenic treatment. *Magn Reson Imaging*. 2015;33:725–736.
59. Li X, Kang H, Arlinghaus LR, et al. Analyzing spatial heterogeneity in DCE- and DW-MRI parametric maps to optimize prediction of pathologic response to neoadjuvant chemotherapy in breast cancer. *Transl Oncol*. 2014;7:14–22.
60. Sutton EJ, Oh JH, Dashevsky BZ, et al. Breast cancer subtype intertumor heterogeneity: MRI-based features predict results of a genomic assay. *J Magn Reson Imaging*. 2015;42:1398–1406.
61. Carlson JJ, Roth JA. The impact of the Oncotype DX breast cancer assay in clinical practice: a systematic review and meta-analysis. *Breast Cancer Res Treat*. 2013;141:13–22.
62. Douglas-Jones AG, Collett N, Morgan JM, Jasani B. Comparison of core oestrogen receptor (ER) assay with excised tumour: intratumoral distribution of ER in breast carcinoma. *J Clin Pathol*. 2001;54:951–955.

**Appendix 1.** Correlation between CT heterogeneity analysis and IHC.

		KI-67	MVD-CD34	CAIX	GLUT-1	HIF-1A	VEGF	SMA
First order	Mean	$r = -0.295$ $P = .286$	$r = 0.325$ $P = .237$	$r = -0.122$ $P = .666$	$r = -0.022$ $P = .939$	$r = -0.371$ $P = .174$	$r = -0.126$ $P = .655$	$r = -0.506$ $P = .054$
	Skewness	$r = -0.341$ $P = .213$	$r = -0.382$ $P = .159$	$r = -0.089$ $P = .751$	$r = 0.012$ $P = .965$	$r = 0.246$ $P = .376$	$r = 0.026$ $P = .928$	$r = 0.391$ $P = .149$
	Kurtosis	$r = -0.431$ $P = .109$	$r = 0.207$ $P = .458$	$r = -0.433$ $P = .107$	$r = -0.463$ $P = .082$	<b><math>r = -0.533^*</math></b> <b><math>P = .041</math></b>	$r = 0.047$ $P = .867$	$r = -0.241$ $P = .386$
	Energy	$r = 0.206$ $P = .462$	$r = 0.311$ $P = .259$	$r = -0.086$ $P = .761$	$r = 0.016$ $P = .955$	$r = -0.203$ $P = .468$	$r = -0.215$ $P = .441$	$r = -0.316$ $P = .251$
	Entropy	$r = -0.198$ $P = .478$	$r = -0.304$ $P = .271$	$r = 0.122$ $P = .666$	$r = -0.029$ $P = .918$	$r = 0.214$ $P = .444$	$r = 0.181$ $P = .52$	$r = 0.334$ $P = .223$
Second-order GLCM	Energy	$r = -0.184$ $P = .511$	$r = 0.164$ $P = .558$	$r = -0.168$ $P = .549$	$r = -0.369$ $P = .176$	$r = -0.288$ $P = .299$	$r = -0.067$ $P = .811$	$r = -0.213$ $P = .447$
Higher order NGTDM	Coarseness	$r = 0.034$ $P = .904$	$r = -0.164$ $P = .558$	$r = 0.122$ $P = .666$	$r = 0.191$ $P = .494$	<b><math>r = 0.54^*</math></b> <b><math>P = .038</math></b>	$r = 0.036$ $P = .897$	$r = -0.027$ $P = .924$
	Contrast	$r = 0.023$ $P = .934$	$r = 0.204$ $P = .466$	$r = -0.071$ $P = .8$	$r = 0.156$ $P = .58$	$r = 0.12$ $P = .67$	$r = -0.064$ $P = .821$	$r = -0.213$ $P = .447$
	Busyness	$r = 0.084$ $P = .766$	$r = -0.34$ $P = .216$	$r = 0.157$ $P = .576$	$r = 0.007$ $P = .981$	$r = 0.01$ $P = .972$	$r = -0.009$ $P = .974$	$r = 0.47$ $P = .077$
Higher order GLRL	Long-run emphasis	$r = 0.409$ $P = .13$	$r = 0.472$ $P = .076$	$r = 0.029$ $P = .919$	$r = -0.095$ $P = .736$	$r = -0.188$ $P = .501$	$r = 0.06$ $P = .831$	<b><math>r = -0.52^*</math></b> <b><math>P = .047</math></b>
Higher order GLSZM	Long-zone emphasis	$r = 0.238$ $P = .394$	$r = 0.443$ $P = .098$	$r = -0.061$ $P = .83$	$r = -0.191$ $P = .494$	$r = -0.54^*$ $P = .038$	$r = 0.204$ $P = .465$	$r = -0.431$ $P = .109$
Fractal analysis	Fractal dimension	$r = -0.148$ $P = .598$	$r = -0.375$ $P = .168$	$r = 0.15$ $P = .593$	$r = 0.18$ $P = .521$	$r = 0.109$ $P = .699$	$r = -0.06$ $P = .831$	$r = 0.613$ $P = .015^*$
	Lacunarity	$r = 0.177$ $P = .528$	<b><math>r = 0.547^*</math></b> <b><math>P = .035</math></b>	$r = 0.032$ $P = .909$	$r = 0.035$ $P = .902$	$r = 0.021$ $P = .942$	$r = -0.129$ $P = .646$	<b><math>r = -0.634^*</math></b> <b><math>P = .011</math></b>

Abbreviations: CAIX, carbonic anhydrase IX; CT, computed tomography; GLCM, grey-level co-occurrence matrix; GLRL, grey-level run-length; IHC, immunohistochemical; MVD, micro-vessel density; NGTDM, neighbourhood grey-tone difference matrix; SMA, smooth muscle actin; VEGF, vascular endothelial growth factor.

$r$  is the Spearman correlation coefficient value;  $P$  is the significance value attached to the Spearman correlation coefficient value.

\*Significant at  $<.05$  level (2-tailed).